

GelMA Hydrogel Loaded with Extracellular Vesicles Derived from Umbilical Cord Mesenchymal Stem Cells for Promoting Cutaneous Diabetic Wound Healing

Lizong Tang, Congrui Zhao, Yufei Liu, Jie Zhou, Yunsheng Dong, Jiaxing Huang, Tingting Yang, Hui Xiao, Dingbin Liu,* Shufang Wang,* and Hong Cai*



Cite This: *ACS Omega* 2023, 8, 10030–10039



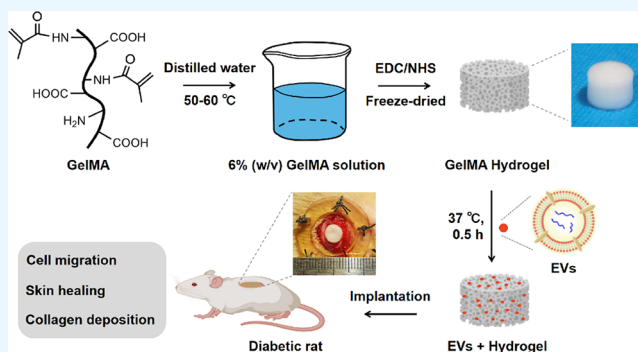
Read Online

ACCESS |

Metrics & More

Article Recommendations

ABSTRACT: Chronic diabetic wounds have become a significant cause of disability worldwide. It is highly desired to develop effective therapies that can promote the rapid healing of diabetic wounds. Owing to the outstanding hydrophilic and water-retaining properties, hydrogels could accelerate the healing process. Extracellular vesicles (EVs) have shown the ability to promote cell regeneration and angiogenesis. In this study, we chose a gelatin methacryloyl (GelMA) hydrogel, a kind of biomaterial characteristic of good biocompatibility, to load the EVs derived from umbilical cord mesenchymal stem cells (UCMSCs) in order to have a long-lasting effect by consistent release of EVs. Then, the hydrogel with EVs was used to treat diabetic wounds in rat models. Nuclear magnetic resonance spectroscopy and scanning electron microscopy were used to characterize the synthesis of the hydrogel; cell experiments, animal experiments, and histological staining were used to evaluate the function of the hydrogel with EVs. The results show that the GelMA hydrogel incorporated with the UCMSC-derived EVs exhibits unique physicochemical properties, excellent biocompatibility, and much enhanced therapeutic effects for diabetic wounds.



INTRODUCTION

Diabetes mellitus is one of the most prevalent chronic diseases in the world. According to the recently released IDF Diabetes Atlas 10th edition report, 537 million adult people are living with diabetes, which means 1 out of 10 people worldwide is suffering from diabetes. It is predicted that 783 million adults will be living with diabetes by 2045.¹ According to a recent survey, the diabetic is accompanied with diverse complications, including chronic ulcers, prolonged inflammation, microvascular disease, and macrovascular disease.^{2–4} Among these complications, diabetic chronic wound brings burden on people due to its high cost and poor outcomes, especially when meeting severe infection, which would probably lead to amputation or even death.⁵ Conventional healing methods, including surgical debridement, graft transplantation, wound dressing, lesion pressure reduction, anti-infection measures, and strict blood glucose control,^{6,7} require lengthy treatment and bring great pains to the patients physically and psychologically. Therefore, it is highly desirable to develop effective therapeutic strategies that could promote wound healing and alleviate the pain of patients simultaneously.

In recent years, a hydrogel has been recognized as an ideal material for wound healing in that its three-dimensional

network structure is similar to a natural soft tissue. In addition, hydrogen can create a high-moisture environment for cells,⁸ allow exchange of oxygen and nutrients, and promote cell proliferation, migration, and differentiation. Due to its excellent performance in promoting wound healing, a variety of hydrogels have been widely used in the field of biomedicine,⁹ some of which have been put into commercial production, hence allowing a lower cost and wider use. At present, there are three main types of raw materials commonly used in hydrogel synthesis,¹⁰ namely, natural materials, synthetic materials, and semisynthetic materials. Gelatin methacryloyl (GelMA), one of the semisynthetic materials, is prepared by chemical modifications that are carried out on natural materials to adjust the physical and chemical properties of the hydrogel to make up for the lack of natural materials.

Received: November 13, 2022

Accepted: February 27, 2023

Published: March 8, 2023



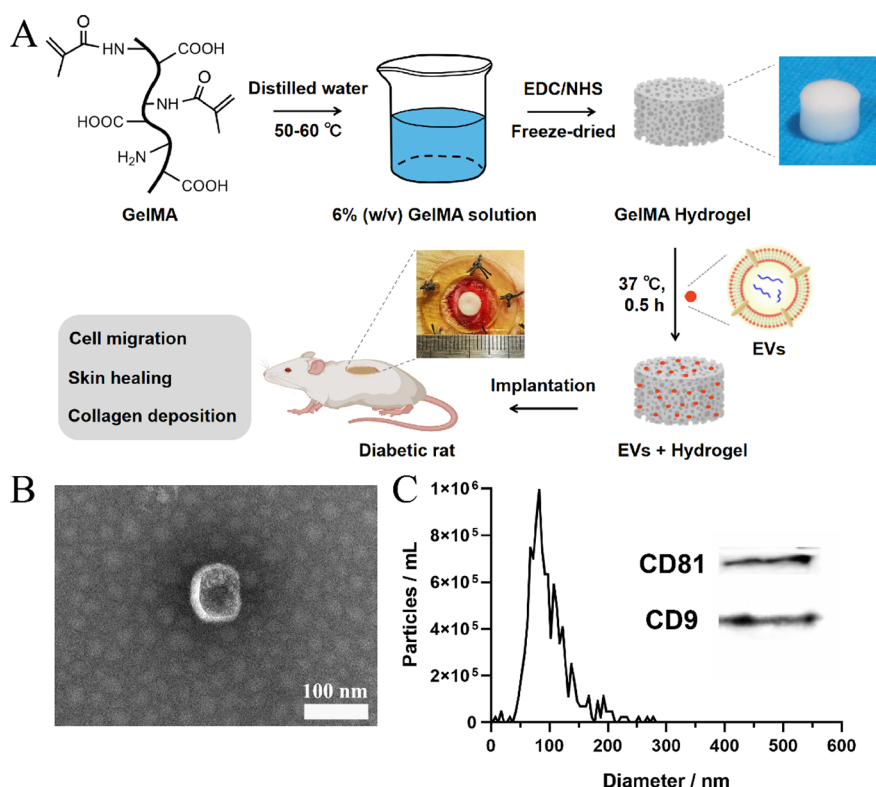


Figure 1. Preparation of the EV-loaded GelMA hydrogel for diabetic wound healing. (A) Schematic of the fabrication process of the EV-loaded GelMA hydrogel and its use for the treatment of diabetic wound. (B) TEM image of the UCMSC-derived EVs. (C) Size distribution of the yielded UCMSC-derived EVs that was measured by NTA. The inset is the Western blot results for the identification of the surface markers (CD81 and CD9) on EVs.

Mesenchymal stem cells (MSCs), such as adipose-derived MSCs,¹¹ bone marrow MSCs,¹² and umbilical cord MSCs (UCMSCs),⁷ have received considerable attention for regenerative therapy,¹³ most likely owing to their multidirectional differentiation potential. However, MSC transplantation treatment may cause problems such as a low transplant survival rate, induction of immunogenicity, and a reduced therapeutic effect.¹⁴ Most recently, extracellular vesicles (EVs) derived from MSCs show high performance for the treatment of skin trauma¹⁵ due to their high therapeutic efficacy but low immunogenicity.¹⁶ EV-based therapy will not only retain the advantages of cell transplantation but also effectively reduce the adverse effects caused by the low survival rate of transplantation.^{17,18} MSC-derived EVs have been applied to various treatments, such as radiation injury, osteoporosis, and skin trauma.^{19,20} However, the EVs derived from UCMSCs for wound healing have not been reported thus far.

In this study, we hypothesized that diabetic wound healing could be accelerated by GelMA hydrogels loaded with UCMSC-derived EVs (Figure 1A). The use of UCMSC-derived EVs would not only prompt healing efficacy but also bring low immune rejection.²¹ The incorporation with GelMA hydrogels offers good biocompatibility and a long-lasting effect by consistent release of EVs. All these advantages suggest that the EV–hydrogel complexes maybe an ideal therapeutic tool for diabetic wound healing.

MATERIALS AND METHODS

Materials. Methacrylic anhydride (MA) was purchased from Sigma (Sigma-Aldrich, St. Louis, Missouri, US). Methacrylic anhydride was from Sigma-Aldrich, St. Louis,

Missouri, US. 1-(3-Dimethylaminopropyl)-3-ethylcarbodiimide hydrochloride (EDC) was from Beijing, China. *N*-Hydroxysuccinimide (NHS) was from Shanghai, China. Paraformaldehyde (4%) was from Shandong, China. A cell counting kit (CCK-8) was purchased from Beyotime Biotechnology Co., Ltd. (Beijing, China). Hematoxylin and eosin (H&E) were purchased from Shandong Sparkjade Biotechnology Co., Ltd. (Shandong, China). Masson's trichrome was purchased from Solarbio Science & Technology Co., Ltd. (Beijing, China).

Synthesis and Characterization of GelMA. GelMA was fabricated according to the outline mentioned in our previous study.²² Briefly, 5 g of porcine skin-derived gelatin (Sigma-Aldrich) was completely dissolved in 50 °C preheated phosphate-buffered saline (PBS), making the solution at a concentration of 10% (w/v). Then, 4 mL of MA was gently added into the gelatin solution with a rate of 0.5 mL/min and stirred for 3 h at 50 °C. The mixture was added with 250 mL of PBS to stop the reaction. Impurities were removed by 7-days dialysis at 40 °C (MW cutoff: 12–14 kDa). The product was placed in a –80 °C freezer followed by lyophilization. Finally, the dry material was stored in a –20 °C freezer sealed as well as protected from light. Gelatin or GelMA (10 mg) was dissolved in 600 μ L of deuterated dimethyl sulfoxide (DMSO), which was then added into a nuclear magnetic tube for structure determination on a nuclear magnetic resonance spectrometer. The synthesis route of GelMA is shown in Figure 2A.

Preparation of GelMA Hydrogels. GelMA hydrogels were fabricated according to a previously reported procedure.²² Briefly, the dry GelMA was fully dissolved in pure

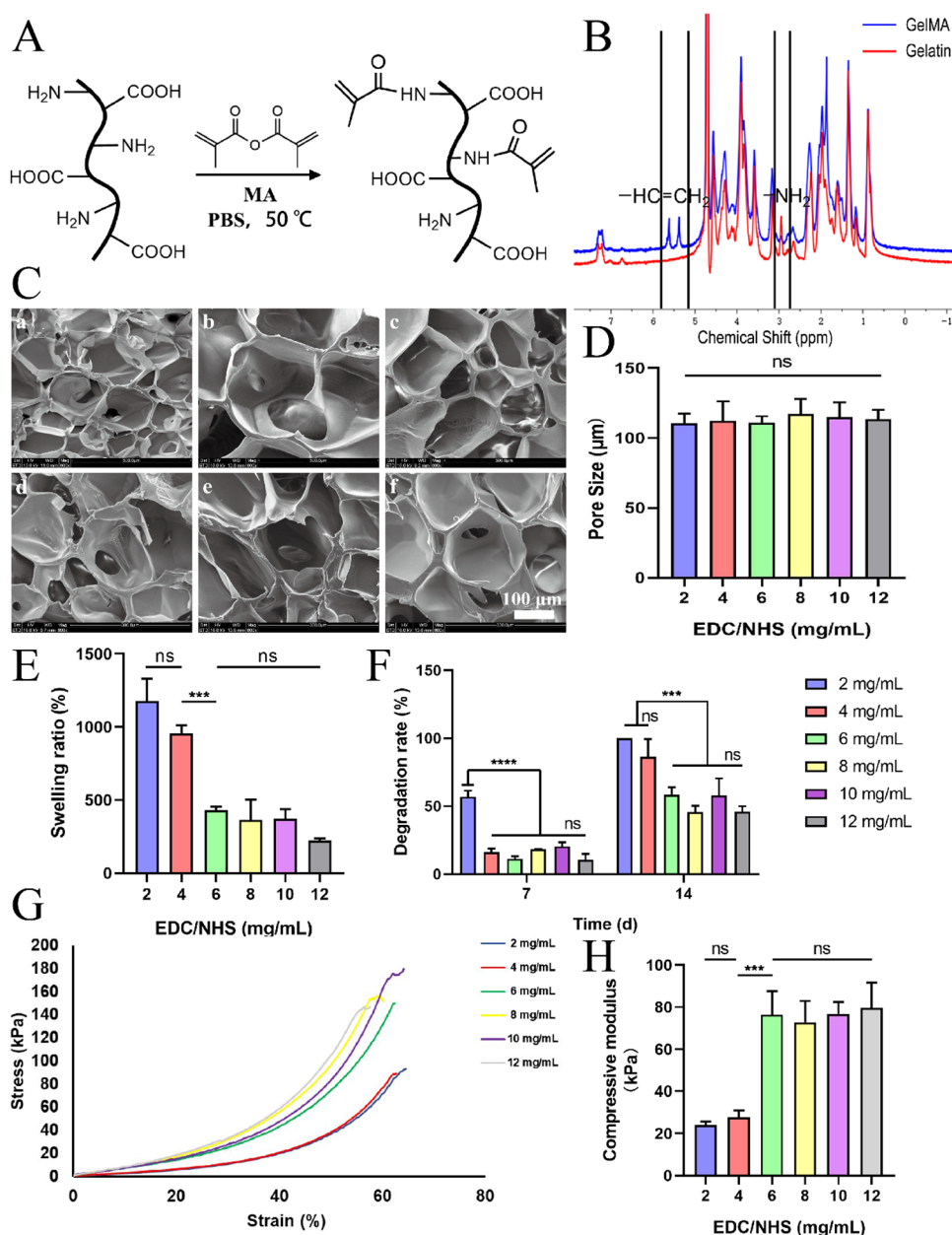


Figure 2. Preparation of GelMA hydrogels and evaluation of their physical properties. (A) Synthesis route of GelMA. (B) ^1H NMR spectra of gelatin and GelMA. (C) SEM images of the hydrogels where GelMA was conjugated with different concentrations of EDC/NHS. (D) Pore sizes and (E) swelling ratios of the hydrogels prepared by GelMA tethering different concentrations of EDC/NHS. (F) Degradation rate about each group of the hydrogels on the 7th and 14th days. (G) Change trend of each group of hydrogels with strain and (H) corresponding compression modulus (* $p < 0.05$, ** $p < 0.01$, *** $p < 0.001$, **** $p < 0.0001$, and $n = 3$).

water at the temperature range of 50–60 °C to achieve a homogeneous solution at a concentration of 6% (w/v). Then, different amounts of EDC/NHS were added to the GelMA solution. Next, the solution was immediately poured into precooled models and then moved to -20 °C for 16 h. Finally, the hydrogels were freeze-dried for 1 day, washed three times with PBS, and freeze-dried again. The dry hydrogels were stored appropriately for further use. The GelMA hydrogel loaded with EVs was prepared by taking a proper amount of EVs, dropped on dry GelMA hydrogels, and then incubated at 37 °C for half an hour.

Characterization of Hydrogels. The freeze-dried hydrogel was cut into pieces with a thickness of about 1 mm; then, conductive glue was used to fix the material on the sample

table for testing. After the gold spray treatment, the internal morphology of each group of hydrogels was observed and photographed by an SEM (FEI Quanta 200, Thermo Fisher Scientific Electron Microscopy, Waltham, MA, USA) after sputter-coating with gold at a voltage of 15 kV. The pore size of each group of hydrogels was counted and analyzed by ImageJ software.

The dried hydrogel was weighed and recorded as W_d and then placed in PBS solution for swelling. After fully swelling at 37 °C for 24 h, the swelled material was weighed and recorded as W_s . By means of formula 1, the swelling rate of each group of hydrogels was calculated:

$$\text{swelling ratio} = \frac{W_s - W_d}{W_d} \times 100\% \quad (1)$$

The lyophilized hydrogel was weighed and recorded as W_0 and then placed in a tube containing 2 mL of PBS at 37 °C for two weeks, during which time the PBS solution was replaced every two days. The samples were freeze-dried and weighed on the 4th, 7th, and 14th days and recorded as W_t . Calculate the degradation rate of the hydrogel sample by [formula 2](#).

$$\text{weight loss} = \frac{W_0 - W_t}{W_0} \times 100\% \quad (2)$$

To determine the hydrophilicity and hydrophobicity of the material, a water contact angle measuring instrument that connects timed capture pictures and real-time video functions was used to measure the water contact angles of GelMA hydrogels at different cross-linking agent concentrations. The data were reported by DrawTool software.

The hydrogel was made into a cylindrical shape and soaked in PBS solution for 24 h to fully swell. After swelling, the diameter and height of the hydrogel were measured to be about 14 and 8 mm, respectively. The fully swollen hydrogel was placed in a universal material testing machine and compressed at a speed of 0.5 mm/min. The stress and deformation were output by a computer. Based on this investigation, the stress–strain curve was drawn, and the compression modulus was calculated from the linear stage from the beginning to the 10% strain.

Isolation and Characterization of EVs. The umbilical cord mesenchymal stem cells (UCMSCs) (ATCC, USA) used in this study were cultured in DMEM (3D FloTrix, CytoNiche, China) supplemented with 100 U mL⁻¹ penicillin–streptomycin (CM0001-100ML, Sparkjade, China) and 10% fetal bovine serum (FBS; Gibco, Australia), and the cells were washed twice with phosphate-buffered saline (PBS; Solarbio, China). The cells were added with medium and cultured for 24 h. Then, the adhered UCMSCs were washed twice with PBS and cultured with basic medium without serum for another 24 h followed by harvesting the EVs from the culture medium.

The culture medium was collected and centrifuged according to a previously reported protocol.²³ In brief, the medium was centrifuged at 300g for 10 min to remove cells, 2000g for 10 min to remove dead cells, 10 000g for 30 min to remove cell debris, and 100 000g for 70 min to remove contaminating proteins. The yielded pellet was washed in PBS at 100 000g for 70 min to enrich the EVs and then resuspended in PBS. All the centrifugation steps were performed at 4 °C.

Using RIPA lysis buffer to lyse the EVs, whose concentrations were determined by a BCA kit, the extracted EVs were stained with a concentration of 20 mg/mL phosphotungstic acid staining solution for 1–2 min at room temperature. The morphology of the EVs was measured with a transmission electron microscope (TEM) after drying. The particle size distribution of EVs was tested using nanoparticle tracking analysis (NTA). EVs were diluted with PBS to an appropriate concentration and added to ZetaView for detection. Eleven sites were detected at the same time, and the measurement was repeated once for each detection site. At the end of the detection, data on particle concentration, particle size, and concentration distribution were obtained. Three replicates were for analyzed for each group. Western blotting was used to detect CD9 and CD81,²⁴ the surface

markers of EVs, and an exposure instrument was used to expose and photograph the results.

Cell Survival and Migration Testing. After fully soaking in a basic medium for 24 h, the hydrogel was filtered and sterilized with a 0.22 μm filter membrane; the extract was stored in a sealed container for later use. L929 mouse fibroblasts were seeded in a 96-well plate at 2000 cells/well; 200 μL of 1640 medium was added and cultured at 37 °C and 5% CO₂ for 1, 2, and 3 days. Four groups were set up in the experiment, namely, the blank control group (B), the hydrogel extract group (H), the EV group (E), and the hydrogel extract plus EV group (H+E), with 3 parallel groups in each group. The concentration of EVs was 20 μg/mL. The CCK-8 experiment was used to obtain the absorbance of each group at a wavelength of 450 nm at different time points and analyze the cell viability.

The L929 mouse fibroblast suspension (200 μL) was inoculated with a density of 1 × 10⁵ cells/mL in the upper chamber of the transwell. Next, the lower chamber was filled with 600 μL of basic culture medium supplemented with hydrogel extract, EV solution, hydrogel extract with EVs, or serum-free medium as a blank control. After a 12 h incubation at 37 °C with 5% CO₂, the transwell chamber was removed, and the cells were fixed with 4% paraformaldehyde. Next, the cells on the upper surface of the membrane were carefully wiped off using a cotton swab, and the migrated cells on the lower surface were stained with 1% crystal violet for 5 min. Finally, a light microscope was used to observe cells and capture images, and then, the number of migrated cells in five randomly selected fields per well was counted.

In Vivo Animal Studies. Construction of a Diabetic Rat Model. Eight-week-old male SD rats (300–350 g) were selected to prepare the diabetic wound models. The rats were kept in the laboratory for one week to adapt to the environment. After the adaptation period, a 10 mg/mL streptozocin (STZ) solution was prepared with normal saline, and the rats were injected intraperitoneally at a dose of 60 mg/kg.²⁵ Three days after the intraperitoneal injection, blood was taken from the tail vein, and blood glucose was measured with a blood glucose meter. When the blood glucose value of the rat was higher than 16.7 mmol/L, accompanied by frequent drinking, frequent meals, polyuria, and weight loss, the model was successfully made.

Construction of Diabetic Rat Trauma. The diabetic model rats were selected for anesthetizing by using isoflurane through an anesthesia machine, and the operation was performed at a concentration of 2–2.5%. The back of the rats was disinfected, and then, a sterilized skin drill was used to create two full-thickness skin wounds with a diameter of 0.8 cm on the skin on both sides of the rat back and spine. A skin fixing ring with an inner diameter of 1.5 cm was employed to reduce the impact of rat skin contraction on wound healing.

Healing Rate Evaluation. After the operation, the wounds were photographed on the 1st day, 3rd day, 7th day, and 14th day. Image processing software Adobe Photoshop was utilized to process the pictures and calculate the wound area and healing rate of each group at different time points.

On the 7th and 14th days after the operation, the rats were killed by intraperitoneal injection of excessive chloral hydrate. The wound and surrounding tissues of about 1 cm were cut out, fixed with paraformaldehyde for 12 h, dehydrated, paraffin-embedded, and finally stored at room temperature for later use.

Histological Analysis. On the 7th and 14th days after the operation, the rats were sacrificed by intraperitoneal injection of excessive chloral hydrate. The wound and surrounding tissues of about 1 cm were cut out, fixed with paraformaldehyde for 24 h, and dehydrated. The wound tissue samples were embedded in paraffin for sectioning into 6 μm -thick sections. The sections were stained with H&E and Masson's trichrome.

Statistical Analysis. GraphPad Prism software was used to analyze the data, which are presented as the mean \pm standard deviation (SD). One-way analysis of variance (ANOVA) was applied to determine the statistical significance of observed differences between the test groups.

RESULTS

Characterization of EVs. Ultracentrifugation was employed to enrich the EVs from the UCMSC culture medium. TEM was used to identify the extracted UCMSC-derived EVs; the results showed that the extracted extracellular vesicles exhibit as a cuplike microstructure, which is unique to EVs (Figure 1B). NTA was employed to verify the size distribution of the UCMSC-derived EVs. The results showed that the major peak in the distribution curve was located at approximately 81 nm, accounting for more than 92.2% of EVs (Figure 1C). Western blotting was further used to detect the expressions of CD9 and CD81, the typical exosomal biomarkers, confirming the successful obtaining of UCMSC-derived EVs.

NMR Characterization of GelMA. Gelatin was conjugated with methacrylic anhydride (MA) to yield GelMA via EDC/NHS chemistry (Figure 2A). The proton nuclear magnetic resonance (^1H NMR) spectra of gelatin and GelMA were collected to evaluate the conjugation (Figure 2B). It can be seen from the figure that there are two peaks at 5.3 and 5.6 ppm in the spectrum of GelMA, which are not found in gelatin. It is inferred that these two peaks belong to methacrylamide, two hydrogens on the carbon-carbon double bond; the peak at 3 ppm of gelatin is lysine methylene, while this peak in GelMA disappears. The result shows the tethering of acrylamide on gelatin, indicating the generation of GelMA.

Characterization of the GelMA Hydrogel. Appearance of the Hydrogel. Figure 2C shows the microstructure of the GelMA hydrogel measured by SEM. It can be observed that the hydrogel has a connected porous structure with uniform pores, which helps the hydrogel to absorb water for swelling. It was reported that ice crystals play a very important role in the formation of the pores; different cross-linking levels should result in pores with different sizes.²⁶ Pore size is an important factor affecting the performance of hydrogels. The high porosity percentage and the interconnected pores of hydrogels are important parameters for achieving high cellular activities including cell penetration, nutrient transport along with the degradation profile, new blood vessel formation, and differentiation.²⁷ The pore size of the freeze-dried hydrogels was counted using ImageJ software. According to the cross-linking agent concentrations from low (2 mg/mL) to high (12 mg/mL), the pore size is determined to be 110.4 ± 6.93 , 112.4 ± 13.82 , 110.8 ± 4.82 , 117.3 ± 10.63 , 114.7 ± 10.91 , and 113.4 ± 6.81 μm . Obviously, the pore size did not change significantly with the increase of the cross-linking agent concentration (Figure 2D).

Swelling Performance of the Hydrogel. In order to explore the influence of the content of the cross-linking agent on the water absorption of the hydrogel, a weighing method was used

to compare the quality of the hydrogel before and after full water absorption and calculate the swelling rate. As shown in Figure 2E, as the concentration of the cross-linking agent increases, the swelling rate of the hydrogel decreases significantly. The swelling rates were determined to be 1176.4 ± 153.3 and $957 \pm 54.07\%$ at the cross-linking agent concentrations of 2 and 4 mg/mL, respectively, and there is no significant difference. The swelling rates of the other four groups with cross-linking agent concentrations ranging from 6 to 12 mg/mL were respectively determined to be 430.169 ± 24.49 , 364.05 ± 139.6 , 373.18 ± 63.73 , and $221.526 \pm 17.02\%$, much lower than those of the 2 and 4 mg/mL groups. There are no statistically significant differences between the four groups at higher concentrations.

It is evident that, as the concentration of cross-linking agent increases, the swelling capability of the hydrogel declines gradually. Combined with results of SEM, this finding is attributed to the increase of pore wall thickness, resulting in variations in the hydrogel's capacity to absorb water. The water-absorbing swelling rate of the hydrogel produced in this experiment was in line with its characteristics, and each group has good water absorption. Upon the hydrogel is applied to wound repair, it could absorb a large amount of exudates and maintain the wetness of the wound surfaces. The healing environment will be more conducive to the proliferation and division of cells at the wound site, thereby helping wound healing.

Characterization of the Hydrogel Stability. The hydrogels of each group were fully immersed in a phosphate-buffered saline solution (pH 6.8) at 37 $^\circ\text{C}$. The degradation rates of the hydrogel were measured at 7 and 14 days, as shown in Figure 2F. On day 7, the lowest cross-linker concentration (2 mg/mL) group had the highest degradation rate, which was determined to be $57.09 \pm 4.3\%$. At the same time, the degradation rates of the rest of the five groups have no appreciable difference, which ranged from 10 to 20%. On day 14, the groups with cross-linking agent contents of 2 and 4 mg/mL had extremely high degradation rates ($>80\%$). Moreover, there was no significant difference between the two low-concentration groups. On the same day, however, the degradation rates of the other four groups dropped to around 50% with no significant difference. The reason for the above phenomenon is presumably due to the higher degree of cross-linking of the hydrogel and the improved stability. It is reasonable that the hydrogel bearing the least amount of the cross-linking agent degrades fastest; it has better degradation performance.

Mechanical Property of the Hydrogel. A universal testing machine was used to evaluate the compression performance of the fully swollen hydrogel. Figure 2G displays the stress change trend for each group of hydrogels under strain together with the compression modulus data. The stress changed slowly with strain at the cross-linking agent concentrations of 2 and 4 mg/mL, resulting in small compressive moduli of 23.93 and 27.63 kPa, respectively. The stress-strain curve trends shown by each group were comparable when the cross-linking agent concentration was 6 mg/mL and higher. The compressive moduli of the four groups from 6 to 12 mg/mL were measured to be 76.41, 72.78, 76.77, and 79.7 kPa, respectively, with no significant difference. It shows that the compressive modulus of the hydrogel is positively associated with the cross-linking agent concentration, but when the cross-linking agent concentration reaches 6 mg/mL and higher, the compressive

modulus tends to be stable and is in the range suitable for skin wound repair.

Gelatin and GelMA were used as biomaterials to make hydrogels at the cross-linking agent concentration of 6 mg/mL, where the as-obtained hydrogels were fully swelled and their compression performance was compared. The results shown in Figure 2H indicate that the stress–strain curves of gelatin and the GelMA hydrogel have similar trends, but the GelMA hydrogel has a better elastic modulus of 76.41 kPa, but the elastic modulus of the gelatin hydrogel is only 53.39 kPa. In contrast, with the same amount of the cross-linking agent, the GelMA hydrogel has more stable mechanical properties, better elasticity and flexibility, and is more suitable as a skin wound repair material.

Evaluation of Cellular Proliferation and Migration.

With the GelMA hydrogels loaded with UCMSC-derived EVs in hand, we used CCK-8 assays to explore their effects on cell proliferation and compared them to those of the prepared hydrogels and EVs alone. The results in Figure 3A show that

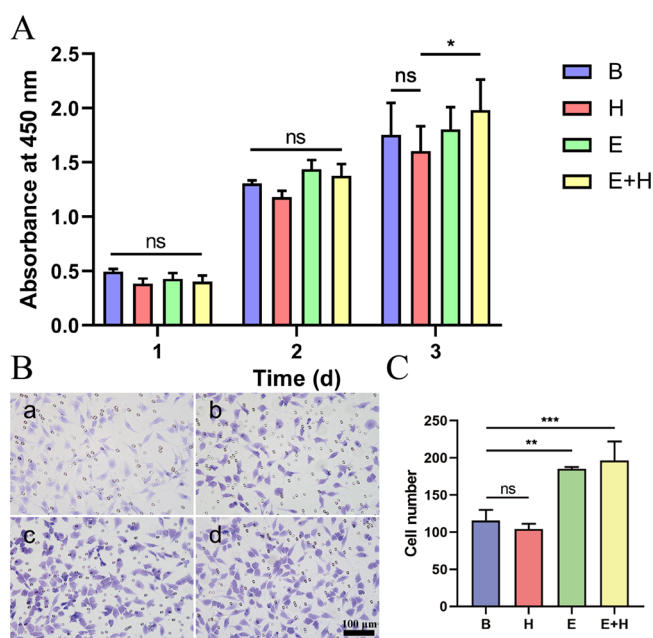


Figure 3. Results of the CCK-8 assay and cell migration assay *in vitro*. (A) CCK-8 assay for L929 cells treated with the hydrogel only (denoted as H), EVs only (denoted as E), and hydrogel extract plus EVs (denoted as E+H) in 3 days. B represents the blank control. (B) Bright images of the HUVEC cell migration assay in different groups (a. blank control; b. hydrogel only; c. EVs only; d. hydrogel extract plus EVs). (C) Quantitative results of the HUVEC cell migration assay in different groups (* $p < 0.05$, ** $p < 0.01$, *** $p < 0.001$, and $n = 3$).

on the first and second days, there was no significant difference in cell proliferation in each group. On the third day, the hydrogel loaded with the EV group showed a promoted effect on cell proliferation. In general, the cell proliferation trend of the hydrogel extract group is not significantly different from that of the blank control group, indicating that the hydrogel has good biocompatibility and no obvious toxicity. The results of the EV group prove that EVs can effectively promote the proliferation of cells, which is beneficial to the proliferation of fibroblasts in the process of wound repair, thereby accelerating the rate of healing.

Figure 3B,C shows the experimental results of cell migration in each group. The results show that the treatment of the hydrogel extract alone has a negligible effect on the cell migration; however, the treatment of UCMSC-derived EVs alone or those incorporated in hydrogels could significantly enhance cell migration. The number of migrated cells treated by EVs is larger than those treated by the hydrogel-only as well as the blank groups (** $p < 0.01$, $n = 3$). In contrast, the EV-loaded hydrogels could induce a greater number of migration cells, showing a much noticeable difference compared to the hydrogel-only as well as the blank groups (*** $p < 0.001$, $n = 3$). These findings show that EVs produced by UCMSCs can promote fibroblast migration, resolving the problem of delayed cell migration in diabetic wounds and assisting in the healing of diabetic wounds.

Evaluation of the Wound Closure Rate, Epidermal Healing, and Collagen Deposit.

We then examined whether the UCMSC-derived EVs could promote diabetic wound closure. We speculated that under *in vivo* conditions, UCMSC-derived EVs may show a high healing effect on wounds due to their functions during the three phases of wound healing, namely, inflammation, proliferation, and remodeling.²⁸ To analyze this, a diabetic chronic wound healing rat model was developed. As shown from the results on the 3rd, 7th, and 14th days after surgery, all the groups have a wound closure trend but with different rates (Figure 4A,B). When treated with the hydrogel or the EV-loaded hydrogel, the cutaneous wound showed a faster closure trend. Even when compared with the nondiabetic control group, the wound healing condition treated with the EV-loaded hydrogel showed a close repair rate. Multiple studies have shown that MSC-EVs are beneficial to the regeneration process of diabetic foot ulcer (DFU), including the inflammation stage, angiogenesis stage, re-epithelialization, and remodeling stage. MiRNAs and proteins, such as nuclear factor erythroid 2-related factor 2 (NRF2) OxOband, miR-21, and miR-23a encapsulated in MSC-EVs, play a vital role in promoting cell proliferation of connective tissues.²⁹ The result suggests that the hydrogel and UCMSC-derived EVs have a synergistically positive effect on wound closure.

To further demonstrate the therapeutic effects, we did histological evaluation of wound tissues after 7 and 14 days of surgery. As shown in Figure 5A, on day 7 after surgery, all groups were infiltrated with inflammatory cells, but fewer inflammatory cells were found in groups treated with the EV-loaded hydrogels. However, at the same time, cutaneous wound still suffers from incomplete recovery, with the absence of the epidermis and the bare dermis. On day 14 after surgery, we noticed a better healing condition, which is characteristic of less inflammatory cells. The skin tissue structure of the nondiabetic control group was basically normal, and the epidermal layer recovered well, while the epidermal layer of the diabetic blank control group did not recover sufficiently. Compared with the blank control group, both the hydrogel and the EV-loaded hydrogel groups were slightly better; the epidermis in the two groups was relatively complete, and the epidermal layer in the EV-loaded hydrogel group was thicker and recovered well.

To sum up, the diabetic wounds treated with the EV-loaded hydrogels recovered better. In Figure 5B, on day 14 after operation, the structure of collagen fibers in the dermis was close to that under the normal condition. Especially in the experimental group treated with EV-loaded hydrogels, the

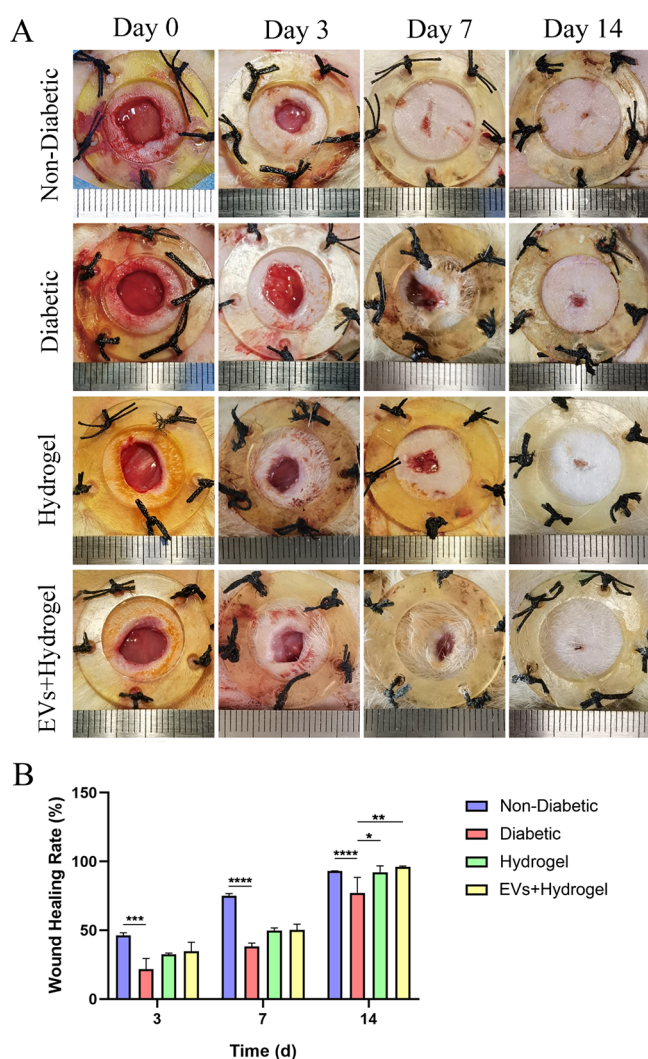


Figure 4. Effect of the EVs/hydrogel on wound healing. (A) Representative images of the wounds in the model mice, which were treated with four therapies, namely, the nondiabetic group, diabetic group, hydrogel, and EVs plus hydrogel, for 14 days. (B) Quantitative analysis of the wound healing rate of each group ($*p < 0.05$, $**p < 0.01$, $***p < 0.001$, $****p < 0.0001$, and $n = 3$).

epidermis was relatively flat, and the collagen deposition was good, which was closer to the recovery of the nondiabetic control group. The quantitative results in Figure 5C,D proved that, on day 7, the collagen deposition level in the EV-loaded hydrogel group was higher than those in the nondiabetic and diabetic groups with significant differences. On day 14, the collagen deposition level in the EV-loaded hydrogels group became the highest among all the groups, including the hydrogel alone group. It shows that the hydrogel constructed in this experiment and its combination with EVs are helpful for the repair of diabetic skin wounds.

DISCUSSION

With the rapid increase in the incidence of diabetes worldwide, the treatment of diabetes and its complications has been paid considerable attention.³⁰ As one of the most common complications of diabetes, chronic diabetic wounds (also known as diabetic ulcers) are difficult to heal, have a long course of disease, and may lead to infection or even local necrosis, ultimately leading to serious consequences of

amputation.³¹ The current clinical treatment plans mostly stay on the relatively old debridement and internal medicine to lower blood sugar.³² The treatment time is long, time-consuming, and laborious, and the treatment process is painful. To solve these problems, scientists have worked out a rich array of methods, like using growth factors³³ and antibacterial dressing.³⁴

This study proposes an integrated formulation by incorporating UCMSC-derived EVs into GelMA hydrogels with enhanced therapeutic efficacy, excellent biocompatibility, and mechanical properties. EDC and NHS act as chemical cross-linking agents to label GelMA with C=C bonds, as confirmed by ¹H NMR spectroscopy. The amide bond is formed through the connection of the carboxyl group and the amino group, where the three-dimensional network structure is formed and the hydrogel is constructed. Moreover, through a series of chemical and physical tests, the most suitable cross-linking agent concentration was selected. The yielded hydrogels showed relatively uniform pore distribution, suitable pore size, excellent swelling performance, suitable hydrophilicity, good mechanical properties, and cytocompatibility, all of which are beneficial to wound repair. Then, the UCMSC-derived EVs were loaded into the hydrogels and applied to treat the diabetic rat trauma model. Healing and treatment effects were analyzed by the healing rate and histological staining.

It was observed by TEM that the extracted nanoscale vesicles had a cuplike structure unique to EVs; the particle size of the extracted EVs was measured to be around 100 nm by dynamic light scattering analysis. The Western blot assay was used to identify the exosomal surface markers, CD9 and CD81. All the characterizations validated that the extracted nanoparticles were typical EVs.

A set of characterizations were performed to evaluate the properties of the as-prepared hydrogels. Since the low-temperature gel formation and ice crystal pore-making methods were used in this experiment, attention should be paid to strictly controlling the cooling rate to ensure uniform and stable pore size. The swelling performance of the GelMA hydrogel shows an inverse trend with the increase of the cross-linking agent concentration. This phenomenon is attributed to the fact that the hydrogel gets tighter at higher concentrations of cross-linking agents, where the hydrogel pore wall becomes thick. Moreover, the concentration of cross-linking agents has a big impact on the hydrogel's stability. The mechanical test proved that, when the cross-linking agent concentration was above 6 mg/mL, the hydrogel achieved a relatively suitable compression performance, and the mechanical properties of the hydrogels were not significantly different from each other. When comparing the mechanical properties of the gelatin hydrogel and the GelMA hydrogel measured under the same cross-linking conditions, the GelMA hydrogel showed better mechanical properties and mechanical stability, thus making it more suitable for skin wound repair.

In vitro cell experiments showed that the hydrogel extract had no effect on cell proliferation. Under the condition of hydrogel extract, the cell proliferation trend displayed by the L929 mouse fibroblast proliferation experiment was not significantly different from that of the blank group. EVs played an important role in promoting cell proliferation. The experimental results showed that the formulation constructed by integrating EVs to GelMA hydrogels can effectively promote cell proliferation. In the cell migration experiments, similar results were observed. The hydrogel alone had a

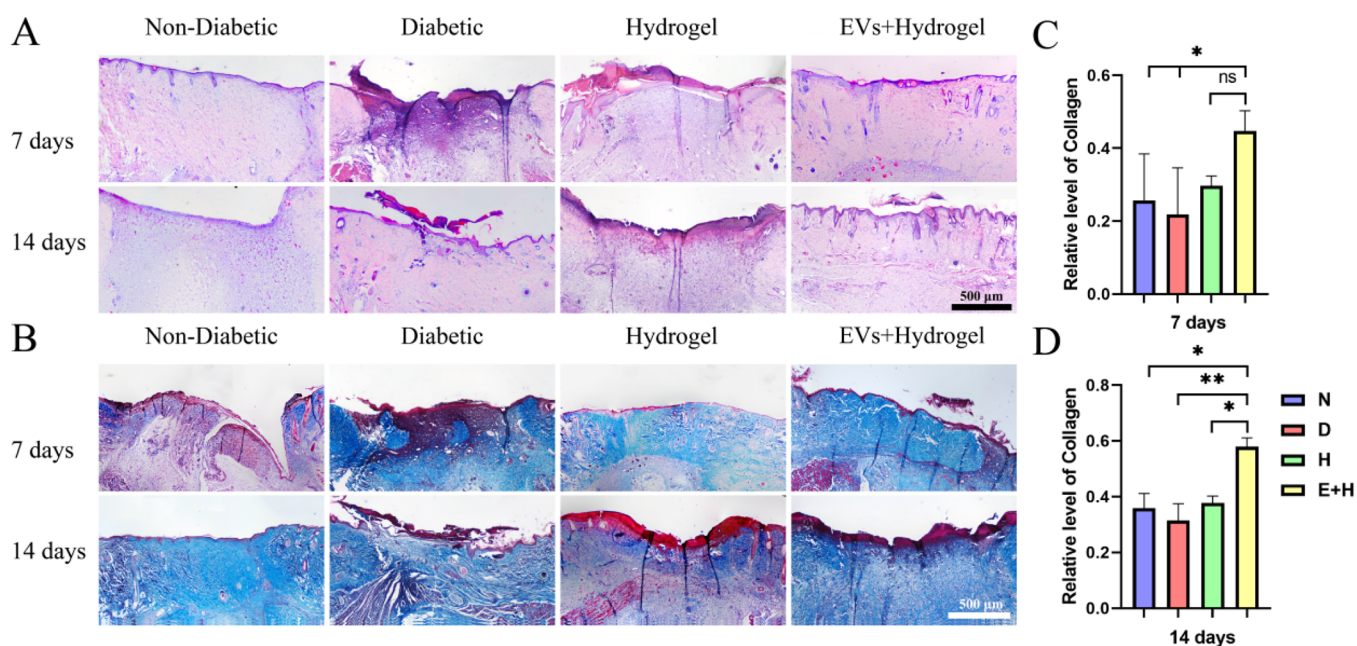


Figure 5. EV-loaded hydrogel increased the wound collagen content and re-epithelialization. (A) Wound sections on days 7 and 14 were stained with hematoxylin and eosin (H&E) for general observation of skin layers. (B) Masson's trichrome staining of skin wound in diabetic mice treated by different groups. Quantitative statistics for collagen deposition on the (C) 7th day and (D) 14th day (* $p < 0.05$, ** $p < 0.01$, and $n = 3$). The scale bar is 500 μm .

negligible effect on the migration of L929 mouse fibroblasts. These investigations proved that the UCMSC-derived EVs can effectively promote the proliferation of fibroblasts and help relieve diabetes especially in combination with hydrogels.

In terms of animal experiments, based on the macroscopic observation of wound images and the statistics of the wound healing rate over time, the treatment effects of both the hydrogel and EV-loaded hydrogel groups were much better than that of the diabetic blank control. It is reasonable that the hydrogel creates a more humid environment for the wound, which was conducive to the migration and proliferation of cells, while the loaded EVs can promote angiogenesis and attenuate the adverse effects of hypoxia on wound repair in the hyperglycemic environment. The results of H&E staining and Masson staining showed that the skin wound healing in the EV-involved group was better, the epidermis was thicker, and the collagen deposition was significantly better than that in the diabetic blank control group 14 days after surgery. It is proven that the addition of EVs can effectively promote the recovery of the epidermal layer and collagen deposition in the diabetic wounds and accelerate the diabetic wound healing.

CONCLUSIONS

In summary, we synthesized a GelMA hydrogel, which was loaded with UCMSC-derived EVs. The as-selected hydrogel has relatively uniform pore distribution, suitable pore size, excellent swelling performance, suitable hydrophilicity, good mechanical properties, and excellent compatibility, all of which are beneficial to wound repair. Then, the EVs secreted by UCMSCs were extracted and loaded into the hydrogel for treating the trauma of the diabetic model rats. Healing and treatment effects were evaluated by recording the healing rate and histological staining. The results confirmed that the hydrogels loaded with UCMSC-derived EVs exhibited a high healing effect on diabetic wounds, providing a new therapeutic tool for wound healing.

AUTHOR INFORMATION

Corresponding Authors

Dingbin Liu – Key Laboratory of Medicinal Chemical Biology, Research Center for Analytical Sciences, Tianjin Key Laboratory of Molecular Recognition and Biosensing, and Institute of Polymer Chemistry, College of Chemistry, Nankai University, Tianjin 300071, China; orcid.org/0000-0003-4153-9822; Email: liudb@nankai.edu.cn

Shufang Wang – Key Laboratory of Bioactive Materials for Ministry of Education, College of Life Sciences, Nankai University, Tianjin 300071, China; orcid.org/0000-0002-0335-6024; Email: wangshufang@nankai.edu.cn

Hong Cai – Department of Dermatology, Air Force Medical Center, PLA, Beijing 100142, P. R. China; Email: ch1031@163.com

Authors

Lizong Tang – Key Laboratory of Bioactive Materials for Ministry of Education, College of Life Sciences, Nankai University, Tianjin 300071, China

Congrui Zhao – Key Laboratory of Bioactive Materials for Ministry of Education, College of Life Sciences, Nankai University, Tianjin 300071, China

Yufei Liu – Key Laboratory of Bioactive Materials for Ministry of Education, College of Life Sciences, Nankai University, Tianjin 300071, China

Jie Zhou – Key Laboratory of Bioactive Materials for Ministry of Education, College of Life Sciences, Nankai University, Tianjin 300071, China

Yunsheng Dong – Key Laboratory of Bioactive Materials for Ministry of Education, College of Life Sciences, Nankai University, Tianjin 300071, China

Jiaying Huang – Key Laboratory of Bioactive Materials for Ministry of Education, College of Life Sciences, Nankai University, Tianjin 300071, China

Tingting Yang – Key Laboratory of Bioactive Materials for Ministry of Education, College of Life Sciences, Nankai University, Tianjin 300071, China

Hui Xiao – Key Laboratory of Bioactive Materials for Ministry of Education, College of Life Sciences, Nankai University, Tianjin 300071, China

Complete contact information is available at:

<https://pubs.acs.org/10.1021/acsomega.2c07291>

Notes

The authors declare no competing financial interest.

ACKNOWLEDGMENTS

This work was financially supported by the National Natural Science Foundation of China (Grant No. 31870966), the National Key Research Development Program of China (2020YFA0803701), the Key Projects of Science and Technology in Tianjin (20YFZCSY01020), and BKJ21J016 and 2021XB008.

REFERENCES

- (1) Sun, H.; Saeedi, P.; Karuranga, S.; Pinkepank, M.; Ogurtsova, K.; Duncan, B. B.; Stein, C.; Basit, A.; Chan, J. C. N.; Mbanya, J. C.; Pavkov, M. E.; Ramachandran, A.; Wild, S. H.; James, S.; Herman, W. H.; Zhang, P.; Bommer, C.; Kuo, S.; Boyko, E. J.; Magliano, D. J. IDF Diabetes Atlas: Global, regional and country-level diabetes prevalence estimates for 2021 and projections for 2045. *Diabetes Res Clin Pract* **2022**, *183*, No. 109119.
- (2) Forbes, J. M.; Cooper, M. E. Mechanisms of diabetic complications. *Physiol Rev* **2013**, *93*, 137–188.
- (3) Harding, J. L.; Pavkov, M. E.; Magliano, D. J.; Shaw, J. E.; Gregg, E. W. Global trends in diabetes complications: a review of current evidence. *Diabetologia* **2019**, *62*, 3–16.
- (4) Jin, X.; Shang, Y.; Zou, Y.; Xiao, M.; Huang, H.; Zhu, S.; Liu, N.; Li, J.; Wang, W.; Zhu, P. Injectable Hypoxia-Induced Conductive Hydrogel to Promote Diabetic Wound Healing. *ACS Appl. Mater. Interfaces* **2020**, *12*, 56681–56691.
- (5) Sloan, G.; Selvarajah, D.; Tesfaye, S. Pathogenesis, diagnosis and clinical management of diabetic sensorimotor peripheral neuropathy. *Nat Rev Endocrinol* **2021**, *17*, 400–420.
- (6) Wang, M.; Wang, C.; Chen, M.; Xi, Y.; Cheng, W.; Mao, C.; Xu, T.; Zhang, X.; Lin, C.; Gao, W.; Guo, Y.; Lei, B. Efficient Angiogenesis-Based Diabetic Wound Healing/Skin Reconstruction through Bioactive Antibacterial Adhesive Ultraviolet Shielding Nanodressing with Exosome Release. *ACS Nano* **2019**, *13*, 10279–10293.
- (7) Yang, J.; Chen, Z.; Pan, D.; Li, H.; Shen, J. Umbilical Cord-Derived Mesenchymal Stem Cell-Derived Exosomes Combined Pluronic F127 Hydrogel Promote Chronic Diabetic Wound Healing and Complete Skin Regeneration. *Int. J. Nanomed.* **2020**, *Volume 15*, 5911–5926.
- (8) Ahmadian, M.; Khoshfetrat, A. B.; Khatami, N.; Morshedloo, F.; Rahbarghazi, R.; Hassani, A.; Kiani, S. Influence of gelatin and collagen incorporation on peroxidase-mediated injectable pectin-based hydrogel and bioactivity of fibroblasts. *J. Biomater. Appl.* **2021**, *36*, 179–190.
- (9) Wang, H.; Xu, Z.; Zhao, M.; Liu, G.; Wu, J. Advances of hydrogel dressings in diabetic wounds. *Biomater. Sci.* **2021**, *9*, 1530–1546.
- (10) Adhya, P.; Sharma, S. S. Redox TRPs in diabetes and diabetic complications: Mechanisms and pharmacological modulation. *Pharmacol. Res.* **2019**, *146*, No. 104271.
- (11) Yin, G.; Yu, B.; Liu, C.; Lin, Y.; Xie, Z.; Hu, Y.; Lin, H. Exosomes produced by adipose-derived stem cells inhibit schwann cells autophagy and promote the regeneration of the myelin sheath. *Int. J. Biochem. Cell Biol.* **2021**, *132*, No. 105921.
- (12) Wang, W.; Zhao, Y.; Li, H.; Zhang, Y.; Jia, X.; Wang, C.; Zhu, P.; Wang, J.; Hou, Y. Exosomes secreted from mesenchymal stem cells mediate the regeneration of endothelial cells treated with rapamycin by delivering pro-angiogenic microRNAs. *Exp. Cell Res.* **2021**, *399*, No. 112449.
- (13) Jin, L.; Wang, X.; Qiao, Z.; Deng, Y. The safety and efficacy of mesenchymal stem cell therapy in diabetic lower extremity vascular disease: a meta-analysis and systematic review. *Cytotherapy* **2022**, *24*, 225–234.
- (14) Liu, W.; Yu, M.; Xie, D.; Wang, L.; Ye, C.; Zhu, Q.; Liu, F.; Yang, L. Melatonin-stimulated MSC-derived exosomes improve diabetic wound healing through regulating macrophage M1 and M2 polarization by targeting the PTEN/AKT pathway. *Stem Cell Res. Ther.* **2020**, *11*, 259.
- (15) Geiger, A.; Walker, A.; Nissen, E. Human fibrocyte-derived exosomes accelerate wound healing in genetically diabetic mice. *Biochem. Biophys. Res. Commun.* **2015**, *467*, 303–309.
- (16) Babaei, M.; Rezaei, J. Application of stem cell-derived exosomes in ischemic diseases: opportunity and limitations. *J Transl Med* **2021**, *19*, 196.
- (17) Xu, R.; Greening, D. W.; Zhu, H. J.; Takahashi, N.; Simpson, R. J. Extracellular vesicle isolation and characterization: toward clinical application. *J Clin Invest* **2016**, *126*, 1152–1162.
- (18) Zhang, X.; Jiang, Y.; Huang, Q.; Wu, Z.; Pu, H.; Xu, Z.; Li, B.; Lu, X.; Yang, X.; Qin, J.; Peng, Z. Exosomes derived from adipose-derived stem cells overexpressing glyoxalase-1 protect endothelial cells and enhance angiogenesis in type 2 diabetic mice with limb ischemia. *Stem Cell Res. Ther.* **2021**, *12*, 403.
- (19) Li, S.; Shao, L.; Xu, T.; Jiang, X.; Yang, G.; Dong, L. An indispensable tool: Exosomes play a role in therapy for radiation damage. *Biomed. Pharmacother.* **2021**, *137*, No. 111401.
- (20) Xu, K.; Zhang, C.; Du, T.; Gabriel, A. N. A.; Wang, X.; Li, X.; Sun, L.; Wang, N.; Jiang, X.; Zhang, Y. Progress of exosomes in the diagnosis and treatment of lung cancer. *Biomed. Pharmacother.* **2021**, *134*, No. 111111.
- (21) Xiang, E.; Han, B.; Zhang, Q.; Rao, W.; Wang, Z.; Chang, C.; Zhang, Y.; Tu, C.; Li, C.; Wu, D. Human umbilical cord-derived mesenchymal stem cells prevent the progression of early diabetic nephropathy through inhibiting inflammation and fibrosis. *Stem Cell Res. Ther.* **2020**, *11*, 336.
- (22) Chen, Y. H.; Rao, Z. F.; Liu, Y. J.; Liu, X. S.; Liu, Y. F.; Xu, L. J.; Wang, Z. Q.; Guo, J. Y.; Zhang, L.; Dong, Y. S.; Qi, C. X.; Yang, C.; Wang, S. F. Multifunctional Injectable Hydrogel Loaded with Cerium-Containing Bioactive Glass Nanoparticles for Diabetic Wound Healing. *Biomolecules* **2021**, *11*, 702.
- (23) Liu, Y.; Zhang, Z.; Wang, B.; Dong, Y.; Zhao, C.; Zhao, Y.; Zhang, L.; Liu, X.; Guo, J.; Chen, Y.; Zhou, J.; Yang, T.; Wang, Y.; Liu, H.; Wang, S. Inflammation-Stimulated MSC-Derived Small Extracellular Vesicle miR-27b-3p Regulates Macrophages by Targeting CSF-1 to Promote Temporomandibular Joint Condylar Regeneration. *Small* **2022**, *18*, No. e2107354.
- (24) Tobon-Aroyave, S. I.; Celis-Mejia, N.; Cordoba-Hidalgo, M. P.; Isaza-Guzman, D. M. Decreased salivary concentration of CD9 and CD81 exosome-related tetraspanins may be associated with the periodontal clinical status. *J. Clin. Periodontol.* **2019**, *46*, 470–480.
- (25) Furman, B. L. Streptozotocin-Induced Diabetic Models in Mice and Rats. *Curr. Protoc. Pharmacol.* **2015**, *70*, 5 471-5 47 20.
- (26) Yuan, Z.; Yuan, X.; Zhao, Y.; Cai, Q.; Wang, Y.; Luo, R.; Yu, S.; Wang, Y.; Han, J.; Ge, L.; Huang, J.; Xiong, C. Injectable GelMA Cryogel Microspheres for Modularized Cell Delivery and Potential Vascularized Bone Regeneration. *Small* **2021**, *17*, No. e2006596.
- (27) Rezaei, F.; Damoogh, S.; Reis, R. L.; Kundu, S. C.; Mottaghitlab, F.; Farokhi, M. Dual drug delivery system based on pH-sensitive silk fibroin/alginate nanoparticles entrapped in PNIPAM hydrogel for treating severe infected burn wound. *Biofabrication* **2021**, *13*, No. 015005.
- (28) Vu, N. B.; Nguyen, H. T.; Palumbo, R.; Pellicano, R.; Fagoonee, S.; Pham, P. V. Stem cell-derived exosomes for wound

healing: current status and promising directions. *Minerva Med* **2021**, *112*, 384–400.

(29) Shiekh, P. A.; Singh, A.; Kumar, A. Exosome laden oxygen releasing antioxidant and antibacterial cryogel wound dressing OxOBand alleviate diabetic and infectious wound healing. *Biomaterials* **2020**, *249*, No. 120020.

(30) Lim, J. Z.; Ng, N. S.; Thomas, C. Prevention and treatment of diabetic foot ulcers. *J. R. Soc. Med.* **2017**, *110*, 104–109.

(31) Pitocco, D.; Spanu, T.; Di Leo, M.; Vitiello, R.; Rizzi, A.; Tartaglione, L.; Fiori, B.; Caputo, S.; Tinelli, G.; Zaccardi, F.; Flex, A.; Galli, M.; Pontecorvi, A.; Sanguinetti, M. Diabetic foot infections: a comprehensive overview. *Eur. Rev. Med. Pharmacol. Sci.* **2019**, *23*, 26–37.

(32) Volmer-Thole, M.; Lobmann, R. Neuropathy and Diabetic Foot Syndrome. *Int. J. Mol. Sci.* **2016**, *17*, 917.

(33) Liu, Y.; Liu, Y.; Deng, J.; Li, W.; Nie, X. Fibroblast Growth Factor in Diabetic Foot Ulcer: Progress and Therapeutic Prospects. *Front. Endocrinol.* **2021**, *12*, No. 744868.

(34) Yang, L.; Liu, F.; Chen, Y.; Liu, Z.; Zhang, G. Research on the Treatment of Diabetic Foot with Ulcer Based on Nano-Silver Antibacterial Dressing. *J. Nanosci. Nanotechnol.* **2021**, *21*, 1220–1229.